Earth and Planetary Science Letters 554 (2021) 116676

Contents lists available at ScienceDirect

Earth and Planetary Science Letters

www.elsevier.com/locate/epsl

Limited iodate reduction in shipboard seawater incubations from the Eastern Tropical North Pacific oxygen deficient zone

D.S. Hardisty [a,*], T.J. Horner [b], N. Evans [c], R. Moriyasu [c], A.R. Babbin [d], S.D. Wankel [b], J.W. Moffett [c], S.G. Nielsen [e]

[a] Department of Earth and Environmental Sciences, Michigan State University, East Lansing, MI, USA
[b] Department of Marine Chemistry and Geochemistry, Woods Hole Oceanographic Institution, Woods Hole, MA, USA
[c] Department of Biological Sciences, University of Southern California, Los Angeles, CA, USA
[d] Department of Earth, Atmospheric, and Planetary Sciences, Massachusetts Institute of Technology, Cambridge, MA, USA
[e] Department of Geology and Geophysics, Woods Hole Oceanographic Institution, Woods Hole, MA, USA

ARTICLE INFO

Article history:
Received 12 May 2020
Received in revised form 26 October 2020
Accepted 8 November 2020
Available online 20 November 2020
Editor: L. Robinson

Keywords:
iodine speciation
oxygen deficient zone
iodate reduction
iodine paleoredox proxy
iodine-to-calcium ratios

ABSTRACT

The relative abundance of the inorganic iodine species, iodide and iodate, are applied to characterize both modern and ancient marine oxygen deficient zones (ODZs). However, the rates and mechanisms responsible for *in situ* iodine redox transformations are poorly characterized, rendering iodine-based redox reconstructions uncertain. Here, we provide constraints on the rates and mechanisms of iodate reduction in the Eastern Tropical North Pacific (ETNP) offshore ODZ using a shipboard tracer–incubation method. Observations of iodate reduction from incubations were limited to the top of the oxycline ($\sigma_\theta \sim 25.2$ kg m^{-3}) where native oxygen concentrations were low, but detectable ($\approx$11 µM). Incubations from additional depths below the oxycline—where O_2 was <2 µM—yielded no detectable evidence of iodate reduction despite hosting the lowest iodate concentrations. These experiments place an upper limit of iodate reduction rates of generally <15 nM day^{-1} but as low as <2.3 nM day^{-1}, which are based on variable precision of individually incubated replicates between experiments. Experimental inferences of limited or slow iodate reduction in the ODZ core relative to that observed in the oxycline are generally consistent with iodate persistence of up to 70 nM and low biological productivity in this zone. We also compare dissolved iodine and oxygen concentrations between variable water masses of the ETNP and globally distributed open ocean ODZs. Consistent with sluggish reduction rates, comparison of iodate concentrations with previously published water mass analyses within the ETNP ODZ ($\sigma_\theta = 26$-27 kg m^{-3}; $O_2 < 7$ µM) demonstrate iodate as a semi-conservative tracer at least partially reflecting regional water mass mixing. A compilation of iodate and dissolved oxygen concentrations from global ODZs generally supports that at least some iodate variations in both vertical and lateral transects largely reflect variable combinations of relatively slow reduction and mixing of iodate reduction signals generated in adjacent regions—as opposed to solely rapid *in situ* processes. In this context, the variations in iodine speciation inferred for the ancient and modern ocean represent a combination of *in situ* processes and regional mixing between water masses that retain variable spatially and temporally integrated redox histories.
© 2020 Elsevier B.V. All rights reserved.

1. Introduction

Iodine serves as a tracer of redox cycling within both modern and ancient marine oxygen deficient zones (ODZs). The reduction of the oxidized inorganic iodine species, iodate (IO_3^-), to the reduced iodide (I^-)—both dissolved in seawater—has a similar Gibbs free energy of reaction and pE to that of the Mn and N redox couples (Farrenkopf et al., 1997a; Rue et al., 1997). In line with these calculations, elevated I^- and corresponding low IO_3^- have been consistently documented within ODZs (Chapman, 1983; Cutter et al., 2018; Farrenkopf and Luther, 2002; Moriyasu et al., 2020; Rapp et al., 2019, 2020; Rue et al., 1997), the oxycline of estuarine low oxygen basins (Luther and Campbell, 1991; Wong and Brewer, 1977), and within anoxic pore waters (Kennedy and Elderfield, 1987a, 1987b; Upstillgoddard and Elderfield, 1988). Building from these field observations, the iodine-to-calcium (I/Ca) paleoredox proxy utility arises from experimental studies demonstrating that IO_3^- incorporates into the carbonate lattice during precipitation whereas I^- does not (Lu et al., 2010). The sole precipitation

* Corresponding author.
E-mail address: hardist1@msu.edu (D.S. Hardisty).

https://doi.org/10.1016/j.epsl.2020.116676
0012-821X/© 2020 Elsevier B.V. All rights reserved.

of calcite with IO_3^- implies that carbonate-bound iodine can be used to trace iodine speciation, and hence, the redox state of ambient waters from which the carbonate precipitated. Applications of I/Ca to track ocean oxygenation cover most of the geologic time spectrum (Hardisty et al., 2017; Hoogakker et al., 2018; Lu et al., 2018).

Modern and ancient applications of iodine to quantitatively track oxygenation depend largely on our understanding of iodine oxidation and reduction in seawater today. The concentration of total inorganic iodine in the ocean is generally conservative near 450-500 nM. Compared to I^- oxidation, the reduction of IO_3^- has been experimentally demonstrated as a potentially rapid process in some low oxygen systems (Amachi et al., 2007; Beck and Bruland, 2000; Farrenkopf et al., 1997b) as well as in oxygenated waters associated with primary production (Hepach et al., 2020). Iodate reduction in oxygenated waters contributes to up to 250 nM I^- found in some euphotic settings and has been linked to both dissimilatory and assimilatory processes during algal growth and senescence (Chance et al., 2014; Hepach et al., 2020). Dissimilatory IO_3^- reduction via bacteria has been demonstrated in experiments under anoxic conditions and inferred to explain near-complete and even quantitative IO_3^- conversion to I^- in ODZ vertical profiles (Farrenkopf et al., 1997b; Amachi et al., 2007). Importantly, though IO_3^- reduction has been documented, IO_3^- formation mechanisms are still not resolved in either low oxygen or well-oxygenated marine settings. It is known that I^- oxidation to form IO_3^-—a six electron transfer—likely involves multiple intermediates, is not directly mediated by oxygen, and tends to be slow compared to rates inferred previously for IO_3^- reduction in both oxic and low oxygen waters (Farrenkopf et al., 1997b; Hepach et al., 2020), but the specific mechanisms, rates, and pathways are still a subject of active research (Chance et al., 2014; Hardisty et al., 2020; Luther et al., 1995). The asymmetry in oxidation-reduction rates could complicate iodine-oxygen relationships, as relatively slow oxidation kinetics may render the persistence of elevated I^- and corresponding low IO_3^- well beyond the locality of *in situ* IO_3^- reduction. A number of studies have also documented elevated I^- within ODZs beyond that possible solely from IO_3^- reduction, including the ETNP, Eastern Tropical South Pacific (ETSP), and Arabian Sea. These ODZs are all inferred to have a shelf pore water I^- source (Cutter et al., 2018; Farrenkopf and Luther, 2002; Moriyasu et al., 2020). Together, relatively slow I^- oxidation kinetics and external sources imply the potential that *in situ* processes need not always govern IO_3^- and I^- accumulation even in low oxygen settings. Indeed, recent detailed transects have revealed that IO_3^- in vertical and lateral profiles appears to be more heterogeneous than previously recognized, both within and between ODZ systems (Cutter et al., 2018; Moriyasu et al., 2020; Rapp et al., 2020).

Experimental constraints on the rates and mechanisms of iodine reduction within ODZ systems are necessary to explain broad field observations and resolve the importance of *in situ* versus transport processes on iodine speciation at a given locality, which have important implications for modern iodine cycling but also the application of the I/Ca paleoredox proxy. To this end, we use shipboard IO_3^- reduction experiments with waters from a vertical transect through the ETNP ODZ. These experiments test the degree to which IO_3^- concentrations and rates of reduction can be linked with *in situ* processes. Importantly, we use multiple methods to confirm our observations and constrain reduction rates. The incubations were inoculated with IO_3^-, but also an I^- tracer with a known $^{129}I/^{127}I$ ratio. This tracer allows us to track IO_3^- reduction via concentration changes and independently through isotopic dilution of the I^- tracer. This study also benefits from complimentary studies from the same ETNP transect that have constrained detailed iodine speciation (Moriyasu et al., 2020) as well as water mass analysis to estimate the fractional contribution of the various water masses encountered during our sampling (Evans et al., 2020), which we use as context for our interpretations.

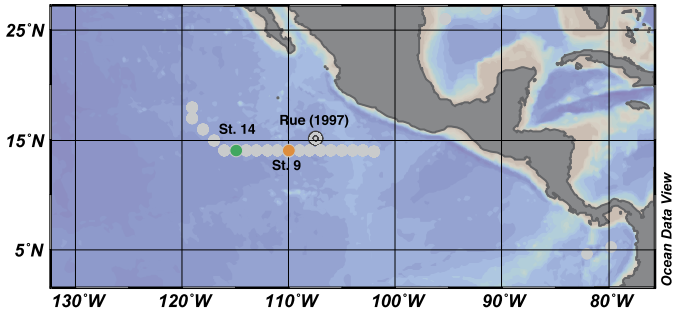

Fig. 1. Map showing transect from FK180624. This figure was created in Ocean Data View. Stations 9 and 14 are the focus of the experimental incubations in this study. Rue et al. (1997) is the location measured previously for iodine speciation. The detailed iodine speciation and water mass analysis, among other chemical parameters, for the FK180624 transect are already published in Moriyasu et al. (2020) and Evans et al. (2020). For context, the iodine speciation, nitrite, and oxygen concentrations are shown in Fig. 2.

2. Sample collection and experimental setup

Samples were collected onboard the R/V *Falkor* at the ETNP ODZ in June and July of 2018 (cruise number FK180624). The samples used for the experiments in this study were collected during an offshore westward transect from 101–120°W centered along 14°N (Fig. 1) where detailed iodine speciation was measured, including at our site, as part of a complementary study (Moriyasu et al., 2020). For the present study, we targeted five depths (95, 105, 145, 168, and 475 m) at 14°N 110°W and one depth (151 m) at 14°N 115°W, which together spanned the ODZ from the lower to upper oxycline and contained native O_2 concentrations ranging from below detection (<1 μM) to ~11 μM (Fig. 1). Because oxygen minima and associated IO_3^- depletion are consistently observed within the 26.2–26.6 kg m^{-3} potential density anomaly range at the ETNP, ETSP, and Arabian Sea (Moriyasu et al., 2020)—and because we ultimately explore water mass mixing as a control on IO_3^- concentrations in this zone—we discuss the experiments in the context of the potential density anomaly to allow for future comparisons between localities.

The sample collection procedure was adapted from that used commonly for experimental studies of nitrogen cycling within ODZs (Fussel et al., 2012; Jensen et al., 2008, 2011). Briefly, seawater from the Niskin bottles was collected within <0.5 h of retrieval into ground-glass reagent bottles and prioritized prior to that necessary for other chemical analyses (Babbin et al., 2014). The bottles were first rinsed 3 × with the sample seawater which was discarded. The bottle was allowed to overflow its volume 3 × while seawater was continuously added. A glass stopper was added so that it displaced seawater at the neck of the bottle. This entire process lasted <5 minutes for each sample collected. The samples were then immediately stored in a refrigerator at 4 °C prior to setting up the experiments which was within 3 h of sample collection.

Unfiltered seawater was used for the experimental incubations at all depths. For 1 depth, 151 m, we performed an additional experiment with 0.2 μm filtered seawater. All tracer addition and seawater aliquoting for the experimental setup was performed in a glove bag flushed with N_2 at 3 × its volume and then episodically flushed throughout the experimental setup (Babbin et al., 2014). For each bottle collected, a pipette was used to remove water from the top at a volume similar to that of the tracer to be added in the subsequent step. A $^{127}IO_3^-$ spike and additional I^- radio-tracer with a known $^{129}I/^{127}I$ ratio (Hardisty et al., 2020)

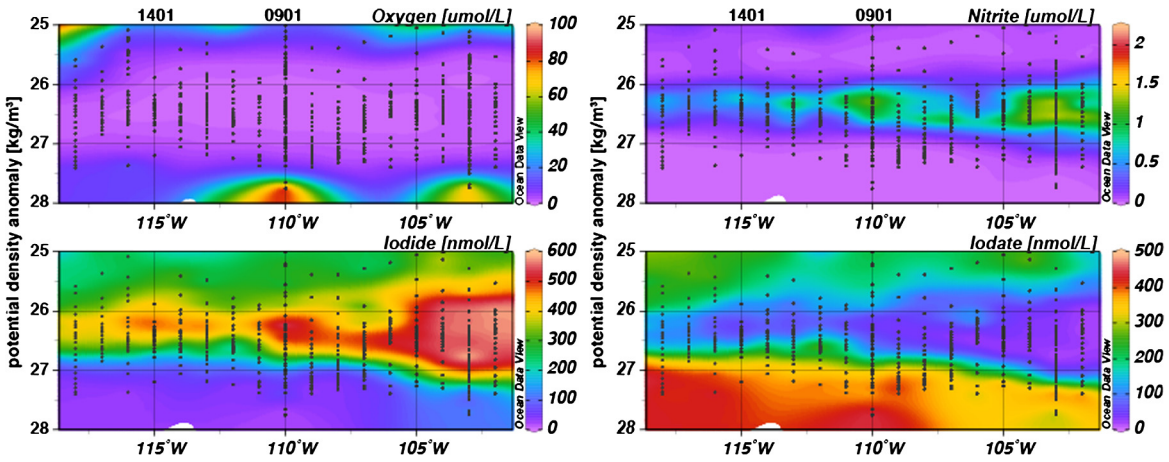

Fig. 2. The oxygen, nitrite, iodide, and iodate concentrations along the *FK*180624 longitudinal transect. Data from Moriyasu et al. (2020). Vertical dots represent points of data collection. The labels at 110°W and 115°W represent Stations 9 and 14, respectively, which were the focus of this study. The y-axis depicts potential density anomaly and focuses on a range displaying the largest iodate gradients. The figure was created in Ocean Data View using weighted-average gridding. (For interpretation of the colors in the figure(s), the reader is referred to the web version of this article.)

were both added separately at levels of ~150 nM $^{127}IO_3^-$ and <80 nM $^{129}I^-$ ($t_{1/2}$ ~ 157 Myrs). In all cases, native $^{129}I^-$ was below detection but $^{127}IO_3^-$ was measurable. The amended seawater was then aliquoted in triplicate into individual 30-60 mL glass serum bottles representing each time point. To remove potential O_2 contamination relicts from the sampling process, the seawater was immediately bubbled for 20-30 minutes with helium through a needle with vented headspace.

The samples were incubated in the dark at 11 °C for up to 60 h. This temperature was chosen to match the temperature range of 8-15 °C measured from the CTD for sample depths evaluated (Supplementary Fig. 1). Triplicate sample bottles were independently incubated for each time point, which varied between incubations but were generally at 0, 12, 24, 48, and 60 h. Upon harvesting, samples were immediately filtered through a 0.2 µm filter and stored in the dark at 4 °C. One fraction of each sample was saved for shipboard total I^- concentration ($^{129}I + {}^{127}I$) measurement and another for $^{129}I/^{127}I$ ratios of I^-. Previous studies have demonstrated iodine stability on the timescales of months to years in filtered seawater and ODZ water (Campos, 1997; Farrenkopf et al., 1997b; Hou et al., 2001; Jickells et al., 1988; Smith et al., 1990). The $^{129}I/^{127}I$ ratios were measured ~3 months following sample collection.

3. Analytical methods

3.1. Iodine speciation

The concentrations of I^- from the incubations were determined shipboard <2 weeks after sample collection via the methods outlined in Moriyasu et al. (2020). Briefly, a 10 mL aliquot of seawater was treated with 150 µL of 0.2% Triton X 100 (Sigma Aldrich – BioX grade) and then purged for 5 minutes with argon gas. Following this, 50 µL of 2 M anhydrous sodium sulfite (Millipore GR ACS) was added to remove O_2 interferences and then purged for an additional minute. Lastly, I^- concentrations were measured with a hanging mercury drop (Hg) electrode and a calomel reference electrode. The I^- concentrations were determined via the method of standard additions to the filtered sample using I^- addition from a KI solution.

Uninoculated seawater samples as well as the t_0 samples for some incubations were characterized for IO_3^-. The IO_3^- was measured via UV-VIS spectrophotometry as described in Moriyasu et al. (2020).

3.2. Iodine chromatographic procedure and isotope ratio quantification

The I^- pool of the seawater was isolated via a recently adapted chromatographic procedure (Hardisty et al., 2020) for measuring the $^{129}I/^{127}I$ ratios of natural waters via accelerator mass spectrometry and inductively coupled plasma mass spectrometry (ICP-MS) (Hou et al., 1999). AG1-X8 resin was used and matrix elution procedures were done according to Hardisty et al. (2020) and I^- was collected via an eluent of 2 M nitric acid-18% (vol/vol) tetramethylammonium hydroxide (TMAH), which was diluted for isotope ratio analysis.

All iodine isotope ratios were measured on a ThermoElectron Neptune multicollector ICP-MS at the Woods Hole Oceanographic Institution Plasma Facility. Iodine was introduced into the MC-ICP-MS as a gas using a sparging technique described previously (Hardisty et al., 2020). Solutions containing 0.5 M nitric acid and 4.5% (vol/vol) TMAH free of iodine were analyzed routinely to monitor contributions from processing blanks and instrument memory. Corrections for instrumental mass bias and isobaric ^{129}Xe were applied as described in Hardisty et al. (2020).

4. Results

The depth profiles for iodine speciation, NO_2^- (nitrite), and O_2 contents determined during the FK180624 transect have been reported previously (Moriyasu et al., 2020; Evans et al., 2020) and are shown here in Fig. 2 plotted against σ_θ. Fig. 3 shows the IO_3^-, I^-, and O_2 concentrations and fluorometer readings relative to depth from sites 9 and 14 along this transect at 110°W and 115°W where the incubation experiments were performed. There is a distinct IO_3^- minimum that corresponds with an I^- and NO_2^- maximum typically within the σ_θ of 25.5–27 kg m^{-3}.

Measured $^{129}I/^{127}I$ ratios of I^- from the incubation experiments are shown in Fig. 4, which reveal little or no variation in $^{129}I/^{127}I$ ratios over the length of the experiments. In Fig. 5, we show the total I^- concentration measured via electrochemistry that includes the native $^{127}I^-$ and the $^{129}I^-$ and $^{127}I^-$ added via the tracer at the onset of the incubations (black circles). In addition, Fig. 5 includes the natural I^- (red squares), which is calculated by determining the total ^{127}I present as I^- in the sample using the $^{129}I/^{127}I$ of I^- measured via MC-ICP-MS and then subtracting the tracer $^{127}I^-$ contribution from this pool based on the added $^{129}I^-$ concentration and the $^{129}I/^{127}I$ ratio of the spike. For the total $^{127}I^-$ (which contains both 'natural' I^- and that from the tracer) concentration calculations, the average total I^- and average $^{129}I/^{127}I$ from

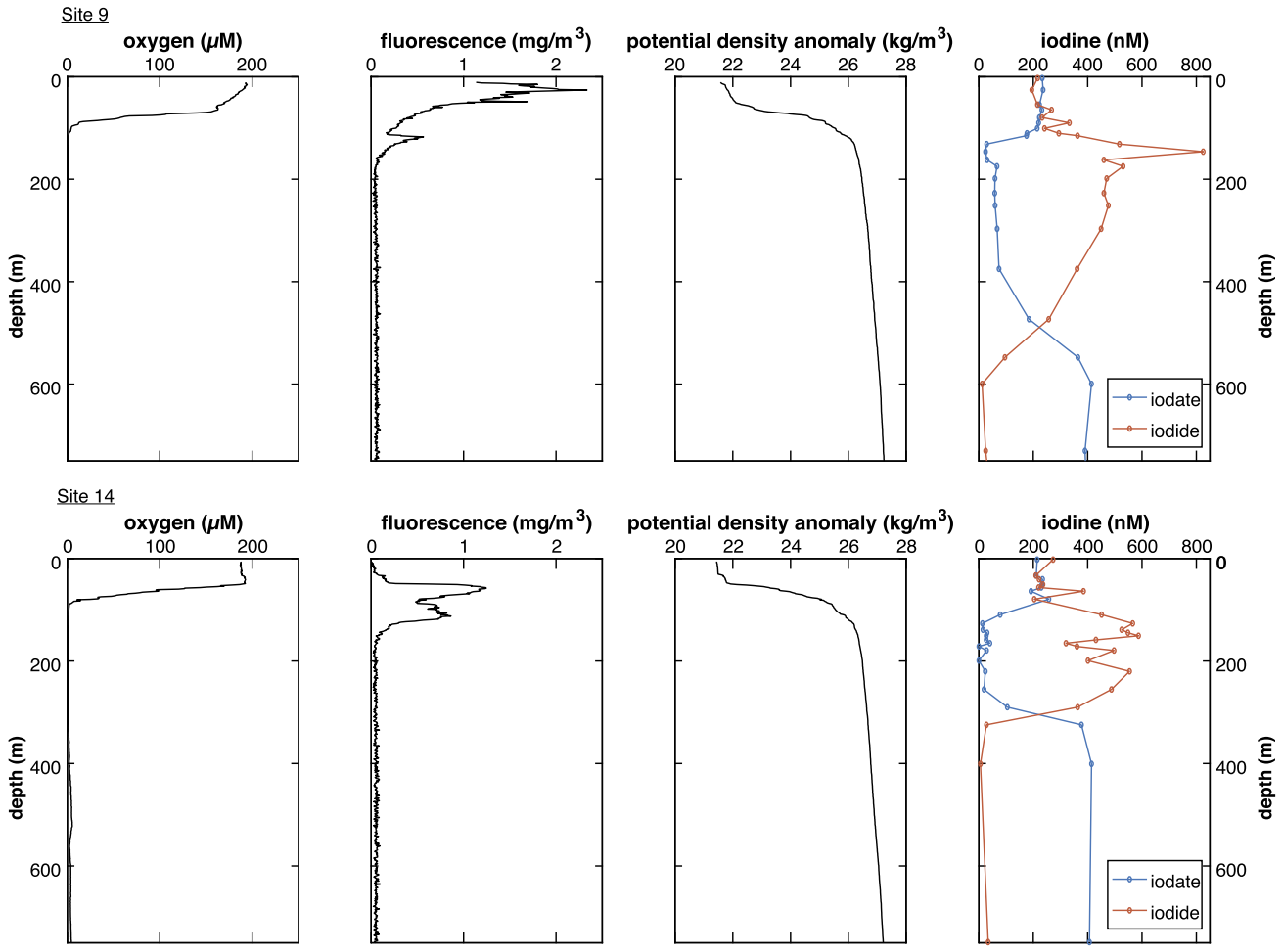

Fig. 3. (a) Oxygen, fluorescence, potential density anomaly, and iodine speciation from site 9 cast 1. Site 9 is located at 110°W. Note that the seawater collected for the incubations at this site came from subsequent casts at this same site (Table 1). (b) Oxygen, fluorescence, potential density anomaly, and iodine speciation from site 14 cast 1 at 115°W. One incubation was performed from seawater at 151 m from this same cast at site 14. These data were published previously in Moriyasu et al. (2020).

the t_0 samples were used to determine and confirm the mass of $^{129}I^-$ added volumetrically prior to the incubations, which are in agreement. Our approach for calculating natural I^- assumes that I^- oxidation was negligible which is likely given the low O_2 conditions, short time frame of the experiments, and known relatively slow I^- oxidation kinetics (Hardisty et al., 2020).

For our experiments, the triplicate time points were incubated, filtered, and measured independently, and their average and standard deviation are shown for each time point. Uncertainties for individual measurements are insignificant relative to the variation between replicate experiments. Hence, mass spectrometric uncertainties do not significantly contribute to total error bars for each time point. For some samples, only duplicates were measured. All raw data are available in Supplementary Table 1.

The shallowest experiment, from 95 m or along the $\sigma_\theta = 25.23$ kg m^{-3}, shows an increase in I^- between the 0 and 24-h time (Fig. 5). The increase in I^- using both the isotopic tracer method and the Hg-electrode method is shown in Table 1. The described trend was observed via both iodine measurement methods. This trend is interpreted to reflect IO_3^- reduction to I^- and this incubation is the only incubation that showed evidence for IO_3^- reduction to I^- (Fig. 5A).

Experiments from deeper depths within the $\sigma_\theta = 25.5$–27 kg m^{-3} did not show changes in I^- outside of repeatability of the experiment's triplicates. As such, we use the standard deviation of the time points within a given experiment to define the limit of detection of I^- changes for each experiment. The maximum detectable increase in I^- concentration varied between experiments (Table 1). The lowest detection limits come from 151 m and 475 m depths, where the $^{129}I/^{127}I$ ratio of I^- constrains the reduction rates to <7.0 and <2.3 nM day^{-1}, respectively. Larger standard deviations for total I^- data generated using the shipboard Hg electrode approach generally yielded lower sensitivity to I^- changes

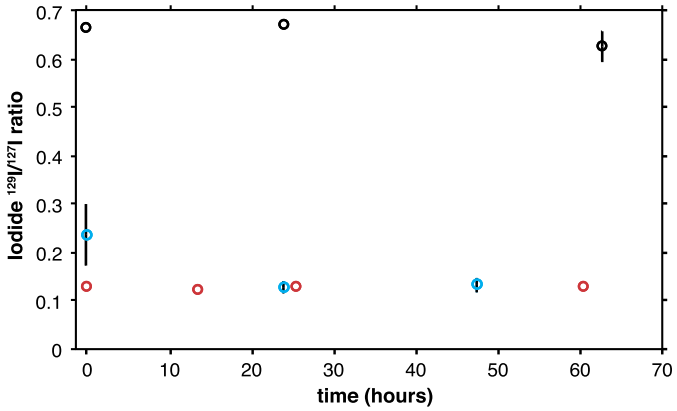

Fig. 4. Shipboard incubations tracking $^{129}I/^{127}I$ of iodide for 95 m or 25.23 kg m^{-3} (blue), 151 m or 25.55 kg m^{-3} (red), and 475 m or 26.93 kg m^{-3} (black). Each of these depths contained native iodide and iodate, which explains differences in initial $^{129}I/^{127}I$ ratios. These isotope data are used to calculate concentration changes, which are shown in Fig. 5. Uncertainties represent one standard deviation of the replicate incubations, which is generally smaller than the data symbols.

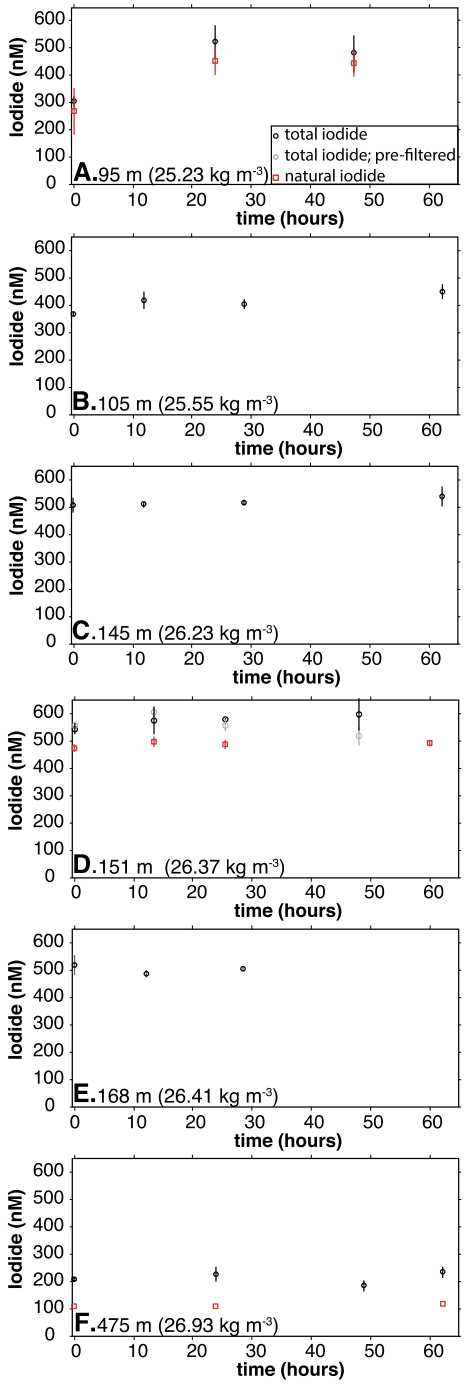

Fig. 5. Shipboard incubations tracking iodate reduction to iodide. For each experiment, ~150 nM iodate was added. As is shown in Figs. 2 and 3, each of these depths also contained native iodate. The black circles represent total I^- ($^{129}I + ^{127}I$) measured shipboard via a Hg-electrode, as explained in the text. The red squares represent select experiments where the $^{129}I/^{127}I$ ratio was measured for I^- and used to quantify natural $^{127}I^-$ concentrations. For one depth, 151 m, an additional 0.2 μm-filtered seawater control experiment was performed alongside the other experiments, which is shown in gray. Data points represent the average of duplicate or triplicate samples independently incubated and measured for each time point. The error bars represent the 1σ of the replicates for each time point.

(11-23.1 nM day^{-1}) than the isotopic approach although both measurement techniques are in good agreement and provide detection limits sufficient for tracking reduction rates observed in previous studies (Amachi et al., 2007; Beck and Bruland, 2000; Councell et al., 1997; Farrenkopf et al., 1997b). In addition, the 0.2 μm-filtered seawater experiment at 151 m is shown in Fig. 5 where it is directly compared with the unfiltered seawater experimental data. The data points for each time point overlap within error for both experiments.

5. Discussion

The ETNP ODZ hosts some of the lowest IO_3^- concentrations in the ocean (Rue et al., 1997; Moriyasu et al., 2020). Coincident with these IO_3^- depletions are significant accumulations of I^- (and NO_2^-; Fig. 2). These features at a given locality represent a mixture of processes occurring locally (i.e., *in situ*) and more broadly within the ODZ (i.e., *ex situ*), the latter transported to our study site(s) via advection. In the following sections, we: (1) examine vertical variations in IO_3^- reduction rates; (2) use the pattern of reduction rates to make inferences regarding the processes responsible; (3) draw on a recently-published statistical decomposition of regional water masses (Evans et al., 2020) to constrain the importance of advection to observed iodine speciation; and, (4) discuss how our results may refine the utility of carbonate I/Ca as a proxy for past redox conditions.

5.1. Iodate reduction is restricted to the upper oxycline

The only experiment with discernable evidence for IO_3^- reduction came from within the upper oxycline of the ODZ (σ_θ = 25.23 kg m^{-3} at 110°W; Fig. 5). The observation of IO_3^- reduction in the upper oxycline of the ODZ is generally consistent with the observed decrease in IO_3^- within this section of our profile (Fig. 2 and 3). Although native O_2 concentrations at this depth were ~11 μM (Fig. 3; Table 1), our experiments were purged with He, which likely altered O_2 to lower values and the O_2 concentration was not monitored, so we cannot directly determine whether IO_3^- reduction is associated with a specific O_2 concentration. For the incubations at this depth, all observed IO_3^- reduction occurred by the first time point (24 h). From this, we determine a minimum IO_3^- reduction rate assuming either a zeroth- (Amachi et al., 2007; Beck and Bruland, 2000) or first-order reaction (Farrenkopf et al., 1997b) of 186 nM day^{-1} and 0.56 day^{-1}, respectively (Table 1). Regardless of the true reaction order, these experiments are the first to confirm IO_3^- reduction within this shallow zone of an ODZ.

Iodate reduction rates were below detection limits for our incubations below the upper oxycline within the σ_θ range of 25.5-27 kg m^{-3} at either 110°W or 115°W (Fig. 5). Detection limits ranged from <2.3 to <23.1 nM day^{-1} depending on the depth, which is based on the standard deviations of experimental replicates (Table 1). This does not directly imply a lack of IO_3^- reduction at these depths or regions of the ETNP ODZ, which could be happening at rates below the sensitivity of our analyses. Indeed, we specifically targeted gradients in IO_3^- while O_2 remained below detection because these features in vertical profiles are typically interpreted to reflect IO_3^- reduction (e.g., Rue et al., 1997). Our lowest detection limits from the experiments come from the 25.5-27 kg m^{-3} σ_θ and put IO_3^- reduction rates at <2.3 nM day^{-1}, <7.0 nM day^{-1}, and <10.2 nM day^{-1} (assuming zeroth order reactions), for 475, 151, and 145 m, respectively (Table 1).

Our observations of limited IO_3^- reduction below the oxycline of the ETNP stand in strong contrast to previous analogous experiments from below the oxycline of the Arabian Sea. In shipboard experiments, Farrenkopf et al. (1997b) report that 200-500 nM IO_3^- added to seawater (a quantity similar to that added in our experiments) was quantitatively reduced to I^- in a series of experiments within six hours. This corresponds to a lower-limit reduction rate estimate of ≥2,000 nM day^{-1}. Additionally, Farrenkopf et al. (1997b) also reported that IO_3^- added to ODZ seawater at levels of ≤1,500 nM—during attempts to create a calibration curve via standard additions—was instantaneously reduced to I^-, implying

Table 1
Estimated upper and lower limits for iodate reduction via the two methods discussed in the main text. The data are plotted in Fig. 5 and are available in Supplementary Table 1. The initial iodate concentrations are that measured for the t_0 samples from the incubations. The 95 m depth native iodate and iodide concentrations were measured from samples collected on a separate cast. The first-order iodate reduction rates consider the initial iodate concentration and the shipboard-derived iodate reduction rate. In some cases the initial or native iodine speciation was not measured (NM).

Station-cast (longitude)	Date started	Depth (m)	Potential density anomaly ($kg\,m^{-3}$)	Native O_2 (μM)	Native iodate (nM)	Native iodide (nM)	Initial iodate (nM)	Iodate reduction rate ($nM\ day^{-1}$)*	Zeroth-order iodate reduction rate ($nM\ day^{-1}$)†	First order iodate reduction rate (day^{-1})*
9-166F (110°W)	July 8	95	25.23	11	206.3	266	388 ± 43	>218.8	>185.7	>0.56
9-03 (110°W)	July 7	105	25.55	2	128.1	356	233 ± 45	<14.5	–	<0.062
9-03 (110°W)	July 7	145	26.23	≤1	33.5	461	91.6 ± 19	<10.2	–	<0.11
14-01 (115°W)	July 11	151	26.34	≤1	26.9	587	NM	<23.1	<7.0	–
9-03 (110°W)	July 7	168	26.41	≤1	61.4	466	153 ± 5.3	<22.1	–	<0.14
9-08 (110°W)	July 9	475	26.93	≤1	368.4	NM	NM	<11.0	<2.3	–

* Rate derived from shipboard total iodide concentration measurements.
† Rate derived from iodine isotope ratio measurements of iodide.

rates far exceeding 2,000 nM day^{-1}. This instantaneous reduction was reported to have occurred in both unfiltered and 0.45 μm-filtered seawater samples and interpreted to be dissimilatory during the oxidation of organic matter. Since there are differences in iodine speciation between the ETNP and Arabian Sea ODZs, we suspect that the different IO_3^- reduction rates observed here and by Farrenkopf et al. (1997b) represent real heterogeneities that are likely not just present between, but also within a given ODZ (i.e., vertically, laterally, temporally). Nonetheless, it is worth noting that there were differences in experimental conditions between our ETNP and the previous Arabian Sea studies. Most prominently, no precautions were taken during sampling to limit O_2 contamination in their shipboard incubations where rapid and quantitative IO_3^- reduction was documented. In contrast, our ETNP sampling protocol and experimental setup included care to both limit and eradicate O_2 contamination, which otherwise would have altered the experiments from natural ODZ conditions. Though it is not currently clear how or if experimental differences might have led to variable iodate reduction rates, we cannot definitively rule this out in the absence of a more detailed study comparing experimental approaches.

The contrasting observations of IO_3^- reduction rates between the ETNP and Arabian Sea are independently supported by important differences in iodine speciation and other characteristics of these ODZ localities. A first difference between the ETNP and Arabian Sea study is that native IO_3^- was frequently observed within the core of the ETNP ODZ at our study locality and throughout the transect (Fig. 2 and 3), while IO_3^- was reported at levels below detection (<20 nM) from the ODZ core in the Arabian Sea when O_2 was below detection (Farrenkopf et al., 1997b). The general presence of IO_3^- within the ETNP ODZ is broadly consistent with relative slower IO_3^- reduction rates, while rapid reduction at the Arabian Sea is consistent with the lack of native IO_3^- above detection in this same zone. If IO_3^- concentrations within the ODZ are at all indicative of expected reduction rates, even slower rates are anticipated for the offshore ETSP, where Cutter et al. (2018) reported O_2 below detection but IO_3^- largely >150 nM in a detailed 18 station ODZ transect covering 70° of longitude westward from the South American margin.

More support for differences in IO_3^- reduction between the ETNP (Moriyasu et al., 2020) and Arabian Sea (Farrenkopf et al., 1997b) studies comes from the fact that the same approach of standard additions was used for the IO_3^- calibration curves in both studies but with contrasting observations. This method includes the shipboard addition of IO_3^- to filtered ODZ seawater samples. Farrenkopf et al. (1997b) reported rapid IO_3^- reduction during this process. In contrast, IO_3^- reduction was not observed during standard additions at the ETNP. These differences provide some independent support for the differences in the experimental results.

5.2. Drivers of iodate reduction

Rapid IO_3^- reduction within the upper oxycline of the ETNP is likely supported by bacteria. Experimental approaches have demonstrated that IO_3^- reduction is a dissimilatory process that can be stimulated under low O_2 conditions as a terminal electron acceptor for microbial-metabolisms oxidizing organic carbon (Amachi et al., 2007; Councell et al., 1997; Farrenkopf et al., 1997b). Iodate reduction has a Gibbs free energy of reaction near $-37\ kJ\,mol^{-1}$ of IO_3^- (Farrenkopf et al., 1997a), thus making it suitable for utilization during bacterial growth. For example, previous studies have shown that both of the marine bacteria *Shewanella putrefaciens* and *Pseudomonas stutzeri* are capable of growth coupled to IO_3^- reduction in artificial seawater under anaerobic conditions (Amachi et al., 2007; Farrenkopf et al., 1997b). Each of these experiments amended IO_3^- concentrations 400 × that of seawater. Though the diversity and distribution of bacteria capable of IO_3^- reduction is not well known, we note that *Pseudomonas* bacteria related to those shown to facilitate IO_3^- reduction have been identified in both the Pacific (Stevens and Ulloa, 2008) and Arabian Sea ODZs (Nair et al., 1994).

The simplest explanation for the difference observed between IO_3^- reduction with depth in our ETNP study relative to rapid IO_3^- reduction in the Arabian Sea is that organic carbon availability—including composition, magnitude, or supply—may play a currently undescribed role in natural variations in IO_3^- reduction rates. Indeed, dissimilatory IO_3^- reduction has already been shown as a function of organic matter type and content in laboratory experiments (Amachi et al., 2007). Though ODZ transects quantifying iodine speciation and IO_3^- reduction have not yet quantified organic carbon availability in the same samples, multiple studies have documented the importance of organic carbon availability for the nitrogen cycle (Ward et al., 2008, 2009; Babbin et al., 2014) which has overlaps in speciation changes with iodine in ODZs (e.g., Fig. 2). Specifically, previous incubation studies have demonstrated that observation of denitrification within the ETNP and ETSP often requires inoculation of an organic substrate (Ward et al., 2008). In contrast, the Arabian Sea is generally more productive with higher experimentally derived denitrification rates occurring even in the absence of organic carbon inoculation (Ward et al., 2008).

Though neither particulate or dissolved organic carbon were measured in our study, some tentative evidence for photosynthetic organic matter production near the oxycline at 95 meters, where IO_3^- reduction was observed (Fig. 5a), comes from relatively elevated chlorophyll-*a* fluorescence readings (Fig. 3) and a corresponding decrease in beam attenuation from the CTD approximating turbidity changes (Supplementary Fig. 1). However, chlorophyll does not necessarily track organic carbon concentrations or export. Additionally, our offshore longitudinal transect did not in-

tersect the shelf where IO_3^- reduction might be more ubiquitous within the ODZ, but it is possible that a similar phenomenon of waning rates from onshore to offshore analogous to the nitrogen cycle (Lam et al., 2011), as related to productivity, could exist for IO_3^-. For example, the low IO_3^- area between the σ_θ range of 25.5-27 kg m^{-3} generally decreases offshore independent of O_2 (Fig. 2). This may reflect a decreasing contribution from either locally active or transported elevated I^- from over the shelf.

Other non-dissimilatory IO_3^- reduction mechanisms are also relevant within ODZ settings. These include reactions with sulfide (Jia-Zhong and Whitfield, 1986) and nitrite (Babbin et al., 2017). The rates of sulfide oxidation via IO_3^- reduction are actually even faster than sulfide oxidation via O_2 (Jia-Zhong and Whitfield, 1986). Intensive sulfur cycling is not a pervasive feature of ODZ water columns, but it has been reported in micro-niches (Canfield et al., 2010; Shanks and Reeder, 1993), transient plumes (Schunck et al., 2013), and directly at the sediment-water interface (Bohlen et al., 2011; Bruchert et al., 2003). Hydrogen sulfide was not measured in this study, but we cannot rule out the possibility that IO_3^- reduction via sulfide is important.

For nitrogen, coupled variability with iodine speciation at the ETNP (Evans et al., 2020; Moriyasu et al., 2020; Rue et al., 1997) and other ODZs (Cutter et al., 2018; Farrenkopf and Luther, 2002) provides some tentative support that these two elemental cycles are linked (Fig. 2). For example, some experiments observed increased NO_2^- oxidation rates with added IO_3^- relative to experiments without added IO_3^-, with inferred IO_3^- reduction rates up to ~17 nM day^{-1} (Babbin et al., 2017). This range is within that detectable for our experiments in the ETNP generally (Table 1) and may still be applicable to our experiments below the oxycline. Future studies should target determining the mechanisms of IO_3^- reduction in ODZs through coupled measurements of nitrogen and sulfur speciation and tracers and controls to infer the role of biological activity.

5.3. Regional processes

Given our constraints placing IO_3^- reduction rates <23.1 nM day^{-1} for the ODZ core (Table 1), which is at least 1 order of magnitude below that observed at the oxycline (>185.7 nM day^{-1}; Table 1, Fig. 5) and at least 2 orders of magnitude relative to the Arabian Sea ODZ (>2000 nM day; Farrenkopf et al., 1997b), we propose that some proportion of the lateral and vertical variations in iodine speciation must be inherited by conservative mixing between water masses. This does not imply that IO_3^- reduction is completely absent in our experiments or in the water column itself. Rather, we suggest the possibility that relatively slow rates in the offshore ETNP ODZ core may allow that water column iodine speciation gradients be sourced from mixing with water masses advected from the shelf where IO_3^- reduction may be stimulated by higher productivity and benthic activity (Farrenkopf et al., 1997a, 1997b; Amachi et al., 2007), reactions with hydrogen sulfide (Jia-Zhong and Whitfield, 1986), or other reductants (Babbin et al., 2017). Similar interpretations have been made for the secondary nitrite maxima of some ODZs (Lam et al., 2011; Sonnerup et al., 2019), a chemical feature that is often coupled to iodine speciation variations (Fig. 2; Moriyasu et al., 2020; Evans et al., 2020). Importantly, this hypothesis for iodine partially links our experimental observations of low rates or absent IO_3^- reduction within the ODZ core with observations of anomalously elevated offshore I^- concentrations within the ETNP, ETSP, and Arabian Sea ODZs that have been inferred as sourced from more highly productive waters overlying the shelf and its associated underlying pore waters (Cutter et al., 2018; Evans et al., 2020; Farrenkopf and Luther, 2002; Moriyasu et al., 2020). In general, the highest ODZ I^- concentrations tend to be centralized near the σ_θ = 26.5 kg m^{-3} (Fig. 2; Moriyasu et al., 2020; Evans et al., 2020). At the ETNP (and ETSP), this σ_θ is partially characterized by the 13 °C water mass (13CW; Peters et al., 2018; Evans et al., 2020). The 13CW is the only ODZ water mass in this region to directly intersect the shelf and has also been linked to pore water I^- inputs into the ETSP (Cutter et al., 2018; Evans et al., 2020; Peters et al., 2018). If IO_3^- reduction within the ODZ is localized to a specific water mass which distributes low IO_3^- waters along its circulation path, the 13CW represents the most likely candidate.

To test the hypothesis that ETNP IO_3^- variability can be explained by some combination of *in situ* processes and water mass exchange, we simulated ETNP IO_3^- concentration by drawing on a recent statistical decomposition of water masses encountered during FK180624 (Evans et al., 2020) and assuming that conservative mixing is the only control on IO_3^- within the ODZ. Under a completely conservative system, a 1:1 linear relationship between simulated and measured IO_3^- is expected, with one of the water masses having an end-member IO_3^- concentration near zero (likely 13CW), explaining the lowest values in the ODZ, and another with an end-member value at or above the highest IO_3^- concentrations observed within the ODZ, ≥495 nmol L^{-1}. Specifically, we utilize here the published ETNP FK180624 transect IO_3^- concentrations (Moriyasu et al., 2020) and water mass fractions that were determined independently of iodine speciation and concentrations (Evans et al., 2020) to calculate the end-member IO_3^- concentrations of prominent water masses via a singular value decomposition analysis in MATLAB. We then simulated IO_3^- within the transect via a mass balance approach by multiplying the end-member IO_3^- concentrations for a given water mass by the fraction of that water mass in a given sample and then summing the IO_3^- contributions from each water mass to each individual sample.

We are focused on processes occurring within the ODZ where IO_3^- reduction was not observed in our experiments, so we have narrowed our comparison to the σ_θ range of 26–27 kg m^{-3}. This σ_θ range is dominated by 13CW, NEPIW (Northern Equatorial Pacific Intermediate Water), and AAIW (Antarctic Intermediate Water; Evans et al., 2020). The O_2 concentrations in these waters were ≤7 µmol L^{-1} while IO_3^- concentrations range from below detection up to 495 nmol L^{-1} (Fig. 2; Fig. 6a). There is no clear relationship between IO_3^- and O_2 within this σ_θ range (Fig. 6a).

The estimated end-member IO_3^- concentration for each 13CW, NEPIW, and AAIW are 18.8 ± 11.8, 187.6 ± 16.8, and 437.5 ± 44.5 nmol L^{-1}, respectively. The simulation provides evidence that, in addition to *in situ* processes, water mass mixing is a major contributor to IO_3^- variability within the σ_θ range of 26-27 kg m^{-3} along the ETNP transect. The assumption of conservative mixing, largely between the 13CW and the AAIW, can explain the majority of the observed IO_3^- range even in the absence of consideration of *in situ* IO_3^- reduction processes. For example, the AAIW water mass has an upper-bound simulated endmember IO_3^- value (when accounting for the uncertainty) of 482 nmol L^{-1}, which is near the highest concentration of IO_3^- of 495 nmol L^{-1} observed in the transect. Further, though there are outliers, Fig. 6b shows a comparison between the simulated and measured IO_3^- along the transects that follow a pseudo-linear fit, which is not expected if *in situ* processes and O_2 concentrations were the major control on IO_3^- throughout the entire transect. The demonstration that a water mass mixing simulation can predict a significant fraction of measured IO_3^- provides additional strong evidence for slow rates of *in situ* reduction relative to that determined previously from other localities.

Importantly, our simulation also demonstrates the importance of IO_3^- reduction. For example, the simple observation that the end-member IO_3^- values for both 13CW and NEPIW are well below the typical IO_3^- values of sub-photic normal-marine oxy-

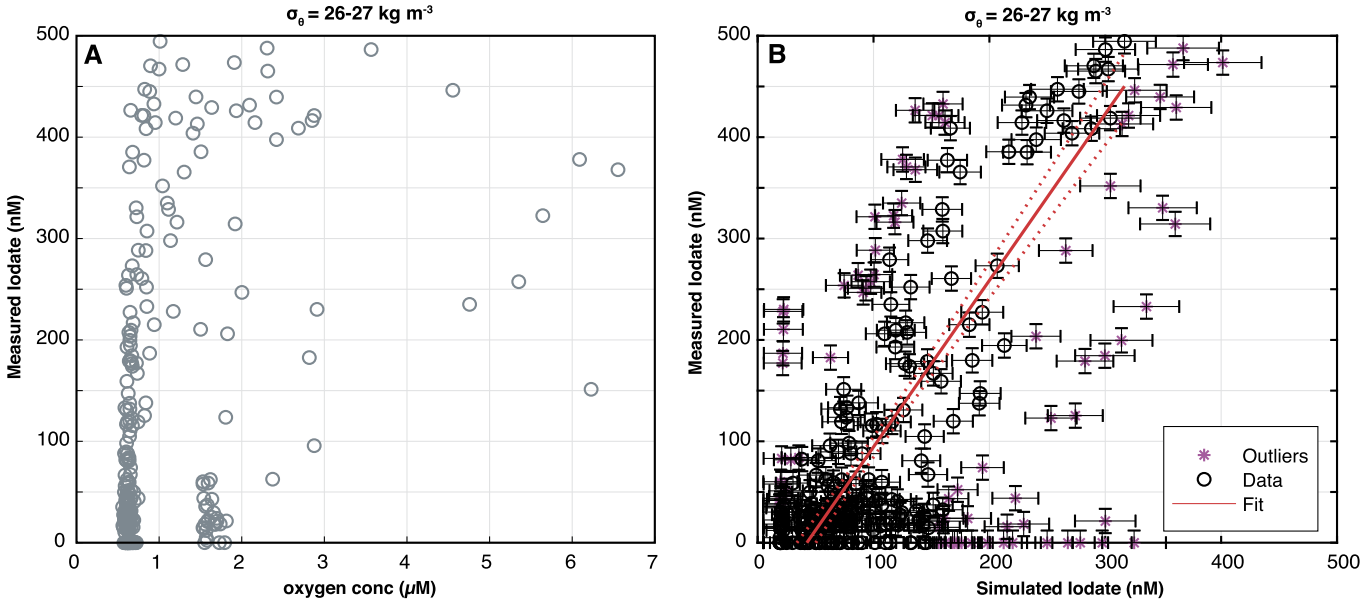

Fig. 6. A. Scatterplot comparison of measured iodate concentration and measured CTD oxygen concentration within the 26-27 kg m^{-3} potential density anomaly range of the FK180624 transect (Fig. 2). **B.** Scatterplot comparison of measured iodate concentration and simulated iodate concentration within the 26-27 kg m^{-3} potential density anomaly range of the FK180624 transect. The regression line represents the best fit of the non-residual data. Outliers are defined as data with iodate concentration >1 standard deviation of the residual. The $r^2 = 0.72$ for non-residual data (n = 197) representing the fit. The $r^2 = 0.38$ for a regression of all available data (not shown, n = 279). The measured iodate data come from Moriyasu et al. (2020) and water mass fractions used to simulate iodate concentrations come from Evans et al. (2020) and include 279 total data points.

genated waters, ~450 nM, and the lowest values in oxygenated euphotic waters—near 250 nM (Chance et al., 2014)—provide evidence for ODZ-related IO_3^- reduction. Specific evidence of ODZ-related IO_3^- reduction within the studied transect region comes from the prevalence of measured IO_3^- values above and below the 1:1 line means that our assumption of a completely conservative system cannot fully explain the measured data (Fig. 6b). For example, outlier data with near-zero measured IO_3^- but with elevated simulated IO_3^- may point to ongoing *in situ* IO_3^- reduction within the 26–27 kg m^{-3} range of the transect but which cannot be simulated with the assumption of conservative mixing. Conversely, the outlier data above the 1:1 line likely represents underestimations of simulated IO_3^- because of the presence and importance of *in situ* processes. We also note that the mass balance simulation failed to produce IO_3^- concentrations >400 nmol L^{-1}, while the highest observed IO_3^- concentrations were near 495 nmol L^{-1}. This result is best explained by the fact that the most IO_3^- enriched water mass, AAIW, accounts for <70% of the contribution to nearly all of the evaluated samples (Evans et al., 2020; Supplementary Fig. 1), hence limiting the potential for simulated IO_3^- concentrations near or equal to its end-member value. This result is likely an artefact of our conservative assumptions and outlines the potential that *in situ* reduction driving the lowest IO_3^- concentrations in some regions may result in underestimations of end-member water mass IO_3^- concentrations.

Lastly, we emphasize that even if iodine speciation is semi-conservative within a given region, it is unlikely to be conservative within or between ODZs on large spatial scales, even if a given water mass is present in multiple ODZs. For example, the 13CW is present in both the ETNP and ETSP, but it is likely highly evolved between the two regions. To compare the IO_3^- concentrations associated with the 13CW between the ETNP and ETSP ODZs, we performed a similar analysis to that described earlier for IO_3^- and water mass fraction using the same types of published data from the σ_θ range of 26-27 kg m^{-3} of the ETSP from GEOTRACES GP16 (Cutter et al., 2018; Peters et al., 2018). The calculations indicate 13CW end-member IO_3^- concentration of ~290 nmol L^{-1} at the

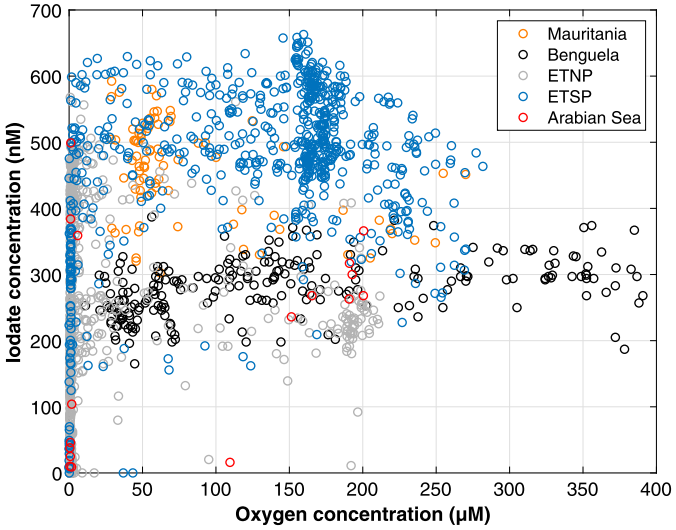

Fig. 7. A comparison of iodate and oxygen concentrations published from global ODZ studies. These include the Mauritania (Rapp et al., 2019), Benguela (Chapman, 1983), Eastern Tropical North Pacific (Rue et al., 1997; Moriyasu et al., 2020), Eastern Tropical South Pacific (Cutter et al., 2018), and the Arabian Sea ODZs (Farrenkopf and Luther, 2002). The detection limits of the O_2 sensors are typically reported near 1 μM.

ETSP which is significantly higher than that obtained for the ETNP (~19 nmol L^{-1}). This difference is consistent with the elevated IO_3^- found in the offshore ETSP ODZ core—IO_3^- generally >150 nM (Fig. 7)—relative to that of the ETNP and likely reflects disparities in *in situ* processes but also generally scales with the variable residence times within the ETNP versus ETSP. Specifically, the O_2 ages have been estimated as ~30 years greater in the ETNP than the ETSP (Karstensen et al., 2008). Future work should focus on determining the localities of, criteria for, and rates of IO_3^- reduction at multiple ODZs in conjunction with water mass ages in an effort to better understand IO_3^- variability within and between these settings.

5.4. Implications for the I/Ca paleoredox proxy

The ranges of I/Ca values in carbonate rocks and foraminifera have been interpreted to reflect combinations of O_2 availability and productivity at the site of carbonate precipitation. Our observations refine these applications, highlighting the importance of low O_2 for IO_3^- reduction and preservation of these signals, but additionally stressing the importance of the regionally integrated redox and productivity and the history of mixing water masses at a given locality. Though I/Ca ratios are not typically interpreted to strictly reflect a corresponding O_2 concentration, the O_2 concentration required to obtain quantitative IO_3^- reduction have been suggested as 25-70 $\mu mol\,L^{-1}$ (Lu et al., 2016), $O_2 < 30\ \mu mol\,L^{-1}$ (Lu et al., 2018), and $\sim 1\ \mu mol\,L^{-1}$ (Hardisty et al., 2014). To further examine the broader validity of IO_3^- as a tracer of local O_2 or a paleoredox tracer, we have compiled IO_3^-–O_2 data from the ODZ literature and consider the observed relationships below in the context of our observations from the ETNP (Fig. 7).

Our compilation of IO_3^-–O_2 from global ODZs in Fig. 7 yields two important findings. First, the presence of significant IO_3^- does not relay specific information regarding the local oxygen levels but is nonetheless a robust indicator of regional oxygenation. Specifically, for each of the ODZs studied, essentially the entire range of IO_3^- observed in the ocean can exist at O_2 concentrations $<7\ \mu mol\,L^{-1}$ (see also Fig. 6a). This is consistent with the importance of water mass mixing in addition to the *in situ* processes of iodine oxidation-reduction in dictating IO_3^- concentrations even at a low O_2 range. However, elevated I/Ca in ancient settings may still represent a strong diagnostic signature of the regional presence of oxic waters regardless of local redox conditions. Given the slow rates observed for I^- oxidation even in well-oxygenated waters (Hardisty et al., 2020), elevated IO_3^- in ODZs is most likely not formed *in situ* but is instead formed in oxygenated waters outside of the ODZ and then preserved due to kinetic constraints on IO_3^- reduction during regional water mass mixing. This interpretation suggests that increases in I/Ca from low baselines in ancient time periods are most consistent with a general broadening of regional oxic marine environments supporting I^- oxidation and IO_3^- preservation or re-organization of ocean circulation pattern favoring IO_3^- at the study site.

Second, IO_3^- concentrations $<150\ nmol\,L^{-1}$ are largely limited to when O_2 concentrations are $<7\ \mu mol\,L^{-1}$. This observation from global ODZs is consistent with independent observations from global oxygenated settings which indicate IO_3^- concentration typically $>250\ nmol\,L^{-1}$ (Chance et al., 2014). This implies that I/Ca values <1.5 μmol/mol in carbonates, or that corresponding to $\sim 150\ nmol\,L^{-1}$ IO_3^- in ambient waters (Lu et al., 2010), may be best interpreted to reflect carbonate precipitation in a water mass with *locally* $O_2 < 7\ \mu mol\,L^{-1}$. This is particularly true of planktonic foraminifera which can be confidently constrained to have spent portions of their life cycle near or within the upper oxycline of an ODZ where we observed active IO_3^- reduction in our experiments. Furthermore, low O_2 concentrations interpreted from I/Ca < 1.5 μmol/mol could be indicative of both active *in situ* IO_3^- reduction, as well as represent a mixture of water masses preserving signatures of IO_3^- reduction along a broader circulation path within low O_2 waters. A similar IO_3^- threshold for interpreting I/Ca values from carbonate precipitation in low O_2 waters was presented in Lu et al. (2016). Importantly though, some previous foraminifera studies have also warned for caution when assigning specific O_2 values based on a given I/Ca value due to decoupling between both I/Ca and IO_3^- relative to ambient O_2 (Lu et al., 2019).

6. Conclusions

We performed shipboard experimental incubations of seawater from a vertical depth transect at an offshore site in the Eastern Tropical North Pacific ODZ in order to provide constraints on IO_3^- reduction rates. We observed reduction at the top of the oxycline where both O_2 and IO_3^- were declining, but IO_3^- reduction was not observed at deeper depths where O_2 was below detection. Our results contribute to a growing number of observations suggesting that ODZ iodine speciation gradients need not always reflect *in situ* processes but can instead partly reflect the mixing of water masses which preserve iodine speciation variations generated elsewhere. Evidence supporting this interpretation includes: **1.** Our observations of low IO_3^- in zones without clear evidence supporting rapid *in situ* IO_3^- reduction; **2.** The persistence of and variations in IO_3^- in the ETNP and ETSP ODZs even when O_2 remains below detection (Cutter et al., 2018; Moriyasu et al., 2020; Rapp et al., 2020); **3.** Comparisons of IO_3^- concentration and water mass fractions within the ETNP ODZ which are consistent with mixing as a control on local iodine speciation, specifically the contributions of the 13CW water mass (Fig. 6; (Evans et al., 2020)); **4.** The common occurrence of elevated offshore I^- concentrations within the σ_θ range of 26-27 $kg\,m^{-3}$ which are linked to transport from coastal pore waters within the ODZ (Cutter et al., 2018; Evans et al., 2020; Farrenkopf and Luther, 2002; Moriyasu et al., 2020). Given these observations, we propose that, beyond our oxycline experiments, IO_3^- reduction may be more prominent in near-shore ODZ settings intersecting the shelf where higher biological productivity and organic carbon can stimulate dissimilatory reduction and benthic reactions possibly with hydrogen sulfide can generate inorganic reduction. In this context, our ETNP observations imply that the iodine speciation at a given ODZ locality can be decoupled from the local O_2 concentrations and hence may more appropriately reflect the integrated redox history of a parcel of water over broad spatial and temporal timescales.

CRediT authorship contribution statement

D.S. Hardisty: Conceptualization; Funding acquisition; Formal analysis; Roles/Writing – original draft. T.J. Horner: Conceptualization; Roles/Writing – Writing – review & editing. N. Evans: Formal analysis; Roles/Writing – Writing – review & editing. R. Moriyasu: Formal analysis; Writing – review & editing. A.R. Babbin: Conceptualization; Resources; Methodology; Writing – review & editing. S.D. Wankel: Conceptualization; Resources; Methodology; Writing – review & editing. J.W. Moffett: Writing – Methodology; review & editing. S.G. Nielsen: Funding acquisition; Conceptualization; Writing – review & editing.

Declaration of competing interest

We confirm that this work is original and has not been published elsewhere nor is it currently under consideration for publication elsewhere. All coauthors have reviewed and approved submission to *EPSL*. We declare no conflicts of interest. Thank you for your consideration.

Acknowledgements

DH and SN acknowledge funding from NSF CO award # 1829406. We thank M. Auro and J. Blusztajn for assistance at the WHOI Plasma Facility. We thank T. Tamasi for assistance with the experimental incubations. The shiptime aboard the R/V *Falkor* was provided by a Schmidt Ocean Institute grant to ARB and Karen Casciotti. ARB also acknowledges financial support from the Simons Foundation (grant 622065) and the Dr. Bruce L. Heflinger and Ally

of Nature funds at MIT. We thank the captain and crew of the R/V *Falkor* for their assistance and for making sample collection possible.

Appendix A. Supplementary material

Supplementary material related to this article can be found online at https://doi.org/10.1016/j.epsl.2020.116676.

References

Amachi, S., et al., 2007. Dissimilatory iodate reduction by marine Pseudomonas sp. strain SCT. Appl. Environ. Microbiol. 73 (18), 5725–5730.

Babbin, A.R., Keil, R.G., Devol, A.H., Ward, B.B., 2014. Organic matter stoichiometry, flux, and oxygen control nitrogen loss in the ocean. Science 344 (6182), 406–408.

Babbin, A.R., et al., 2017. Multiple metabolisms constrain the anaerobic nitrite budget in the Eastern Tropical South Pacific. Glob. Biogeochem. Cycles 31 (2), 258–271.

Beck, N.G., Bruland, K.W., 2000. Diel biogeochemical cycling in a hyperventilating shallow estuarine environment. Estuaries 23 (2), 177–187.

Bohlen, L., et al., 2011. Benthic nitrogen cycling traversing the Peruvian oxygen minimum zone. Geochim. Cosmochim. Acta 75 (20), 6094–6111.

Bruchert, V., et al., 2003. Regulation of bacterial sulfate reduction and hydrogen sulfide fluxes in the central Namibian coastal upwelling zone. Geochim. Cosmochim. Acta 67 (23), 4505–4518.

Campos, M.L.A., 1997. New approach to evaluating dissolved iodine speciation in natural waters using cathodic stripping voltammetry and a storage study for preserving iodine species. Mar. Chem. 57 (1–2), 107–117.

Canfield, D.E., et al., 2010. A cryptic sulfur cycle in oxygen-minimum-zone waters off the Chilean coast. Science 330 (6009), 1375–1378.

Chance, R., Baker, A.R., Carpenter, L., Jickells, T.D., 2014. The distribution of iodide at the sea surface. Environ. Sci. Process. Impacts 16, 1841–1859.

Chapman, P., 1983. Changes in iodine speciation in the Benguela current upwelling system. Deep-Sea Res., A, Oceanogr. Res. Pap. 30 (12), 1247–1259.

Councell, T.B., Landa, E.R., Lovley, D.R., 1997. Microbial reduction of iodate. Water Air Soil Pollut. 100 (1–2), 99–106.

Cutter, G.A., Moffett, J.G., Nielsdóttir, M.C., Sanial, V., 2018. Multiple oxidation state trace elements in suboxic waters off Peru: in situ redox processes and advective/diffusive horizontal transport. Mar. Chem. 201, 77–89.

Evans, N., et al., 2020. The role of water masses in shaping the distribution of redox active compounds in the Eastern Tropical North Pacific oxygen deficient zone and influencing low oxygen concentrations in the eastern Pacific Ocean. Limnol. Oceanogr.

Farrenkopf, A.M., Luther III, G.W., Truesdale, V.W., Van der Weijden, C.H., 1997a. Sub surface iodide maxima: evidence for biologically catalyzed redox cycling in Arabian Sea OMZ during the SW intermonsoon. Deep-Sea Res., Part 2, Top. Stud. Oceanogr. 44 (6–7), 1391–1409.

Farrenkopf, A.M., Dollhopf, M.E., Chadhain, S.N., Luther III, G.W., Nealson, K.H., 1997b. Reduction of iodate in seawater during Arabian Sea shipboard incubations and in laboratory cultures of the marine bacterium Shewanella putrefaciens strain MR-4. Mar. Chem. 57 (3), 347–354.

Farrenkopf, A.M., Luther, G.W., 2002. Iodine chemistry reflects productivity and denitrification in the Arabian Sea: evidence for flux of dissolved species from sediments of western India into the OMZ. Deep-Sea Res., Part 2, Top. Stud. Oceanogr. 49 (12), 2303–2318.

Fussel, J., et al., 2012. Nitrite oxidation in the Namibian oxygen minimum zone. ISME J. 6 (6), 1200–1209.

Hardisty, D., Horner, T., Wankel, S., Blusztajn, J., Nielsen, S., 2020. Experimental observations of marine iodide oxidation using a novel sparge-interface MC-ICP-MS technique. Chem. Geol. 532, 119360.

Hardisty, D.S., et al., 2017. Perspectives on Proterozoic surface ocean redox from iodine contents in ancient and recent carbonate. Earth Planet. Sci. Lett. 463, 159–170.

Hardisty, D.S., et al., 2014. An iodine record of Paleoproterozoic surface ocean oxygenation. Geology 42, 619–622.

Hepach, H., Hughes, C., Hogg, K., Collings, S., Chance, R., 2020. Senescence as the main driver of iodide release from a diverse range of marine phytoplankton. Biogeosciences 17, 2453–2471.

Hoogakker, B.A.A., et al., 2018. Glacial expansion of oxygen-depleted seawater in the eastern tropical Pacific. Nature 562 (7727), 410–413.

Hou, X., Dahlgaard, H., Nielsen, S., 2001. Chemical speciation analysis of 129 I in seawater and a preliminary investigation to use it as a tracer for geochemical cycle study of stable iodine. Mar. Chem. 74 (2), 145–155.

Hou, X., et al., 1999. Determination of chemical species of iodine in seawater by radiochemical neutron activation analysis combined with ion-exchange preseparation. Anal. Chem. 71 (14), 2745–2750.

Jia-Zhong, Z., Whitfield, M., 1986. Kinetics of inorganic redox reactions in seawater: I. The reduction of iodate by bisulphide. Mar. Chem. 19, 121–137.

Jensen, M.M., Kuypers, M.M.M., Lavik, G., Thamdrup, B., 2008. Rates and regulation of anaerobic ammonium oxidation and denitrification in the Black Sea. Limnol. Oceanogr. 53 (1), 23–36.

Jensen, M.M., et al., 2011. Intensive nitrogen loss over the Omani Shelf due to anammox coupled with dissimilatory nitrite reduction to ammonium. ISME J. 5 (10), 1660–1670.

Jickells, T.D., Boyd, S.S., Knap, A.H., 1988. Iodine cycling in the Sagasso Sea and the Bermuda inshore waters. Mar. Chem. 24 (1), 61–82.

Karstensen, J., Stramma, L., Visbeck, M., 2008. Oxygen minimum zones in the eastern tropical Atlantic and Pacific oceans. Prog. Oceanogr. 77 (4), 331–350.

Kennedy, H., Elderfield, H., 1987a. Iodine diagenesis in non-pelagic deep-sea sediments. Geochim. Cosmochim. Acta 51 (9), 2505–2514.

Kennedy, H., Elderfield, H., 1987b. Iodine diagenesis in pelagic deep-sea sediments. Geochim. Cosmochim. Acta 51 (9), 2489–2504.

Lam, P., et al., 2011. Origin and fate of the secondary nitrite maximum in the Arabian Sea. Biogeosciences 8 (6), 1565–1577.

Lu, W., et al., 2018. Late inception of a resiliently oxygenated upper ocean. Science 361, 174–177.

Lu, Z., et al., 2016. Oxygen depletion recorded in upper waters of the glacial Southern Ocean. Nat. Commun. 7.

Lu, Z., Jenkyns, H.C., Rickaby, R.E., 2010. Iodine to calcium ratios in marine carbonate as a paleo-redox proxy during oceanic anoxic events. Geology 38 (12), 1107–1110.

Lu, W., Dickson, A.J., Thomas, E., Rickaby, R.E., Chapman, P., Lu, Z., 2019. Refining the planktic foraminiferal I/Ca proxy: results from the southeast Atlantic Ocean. Geochim. Cosmochim. Acta.

Luther, G.W., Campbell, T., 1991. Iodine speciation in the water column of the Black Sea. Deep-Sea Res., A, Oceanogr. Res. Pap. 38, S875–S882.

Luther, G.W., Wu, J., Cullen, J.B., 1995. Redox chemistry of iodine in seawater: frontier molecular orbital theory considerations. Aquat. Chem., Interfacial Interspecies Process. 244, 135.

Moriyasu, R., Evans, N., Bolster, K.M., Hardisty, D.S., Moffett, J.W., 2020. The distribution and redox speciation of iodine in the Eastern Tropical North Pacific. Glob. Biogeochem. Cycles.

Nair, S., Loka Bharathi, P.A., Chandramohan, D., 1994. Cultureable bacteria from the euphotic zone the Indian Ocean during the summer monsoon. Oceanol. Acta 17, 63–68.

Peters, B.D., et al., 2018. Water mass analysis of the 2013 US GEOTRACES eastern Pacific zonal transect (GP16). Mar. Chem. 201, 6–19.

Rapp, I., Schlosser, C., Menzel Barraqueta, J.L., Wenzel, B., Lüdke, J., Scholten, J., Gasser, B., Reichert, P., Gledhill, M., Dengler, M., Achterberg, E.P., 2019. Controls on redox sensitive trace metals in the Mauritanian oxygen minimum zone. Biogeosciences 16 (21), 4157–4182.

Rapp, I., Schlosser, C., Browning, T.J., Wolf, F., Le Moigne, F.A., Gledhill, M., Achterberg, E.P., 2020. El Niño-driven oxygenation impacts Peruvian shelf iron supply to the South Pacific Ocean. Geophys. Res. Lett. 47 (7), e2019GL086631.

Rue, E.L., Smith, G.J., Cutter, G.A., Bruland, K.W., 1997. The response of trace element redox couples to suboxic conditions in the water column. Deep-Sea Res., A, Oceanogr. Res. Pap. 44 (1), 113–134.

Schunck, H., Lavik, G., Desai, D.K., Großkopf, T., Kalvelage, T., Löscher, C.R., Paulmier, A., Contreras, S., Siegel, H., Holtappels, M., Rosenstiel, P., 2013. Giant hydrogen sulfide plume in the oxygen minimum zone off Peru supports chemolithoautotrophy. PLoS ONE 8 (8).

Shanks, A.L., Reeder, M.L., 1993. Reducing microzones and sulfide production in marine snow. Mar. Ecol. Prog. Ser. 96 (1), 43–47.

Smith, J.D., Butler, E.C., Airey, D., Sandars, G., 1990. Chemical properties of a low-oxygen water column in Port Hacking (Australia): arsenic, iodine and nutrients. Mar. Chem. 28 (4), 353–364.

Sonnerup, R.E., Chang, B.X., Warner, M.J., Mordy, C.W., 2019. Timescales of ventilation and consumption of oxygen and fixed nitrogen in the eastern tropical South Pacific oxygen deficient zone from transient tracers. Deep-Sea Res., A, Oceanogr. Res. Pap. 151, 103080.

Stevens, H., Ulloa, O., 2008. Bacterial diversity in the oxygen minimum zone of the eastern tropical South Pacific. Environ. Microbiol. 10 (5), 1244–1259.

Upstillgoddard, R.C., Elderfield, H., 1988. The role of diagenesis in the estuarine budgets of iodine and bromine. Cont. Shelf Res. 8 (4), 405–430.

Ward, B.B., Tuit, C.B., Jayakumar, A., Rich, J.J., Moffett, J., Naqvi, S.W.A., 2008. Organic carbon, and not copper, controls denitrification in oxygen minimum zones of the ocean. Deep-Sea Res., A, Oceanogr. Res. Pap. 55 (12), 1672–1683.

Ward, B.B., Devol, A.H., Rich, J.J., Chang, B.X., Bulow, S.E., Naik, H., Pratihary, A., Jayakumar, A., 2009. Denitrification as the dominant nitrogen loss process in the Arabian Sea. Nature 461 (7260), 78–81.

Wong, G.T., Brewer, P.G., 1977. The marine chemistry of iodine in anoxic basins. Geochim. Cosmochim. Acta 41 (1), 151–159.